RESEARCH PAPER

Coupled transient saturated–unsaturated seepage and limit equilibrium analysis for slopes: influence of rapid water level changes

Aynaz Biniyaz[1] · Behnam Azmoon[1] · Zhen Liu[1]

Abstract

This study investigates the influence of the water level fluctuation on the stability of soil slopes using coupled seepage and slope stability analysis. A simulation framework was proposed and implemented seamlessly using Python code to seek insights into three factors that have not been thoroughly studied for this issue: soil unit weight variation in the unsaturated zone, unsaturated shear strength models, and velocity of water drawdown. For this purpose, the seepage analysis was carried out by discretizing a numerical seepage analysis model using a finite element analysis platform, FEniCS. The output of the seepage analysis, i.e., pore water pressure distribution, was used as input for the slope stability analysis. Limit equilibrium methods including the Bishop Simplified method and the Ordinary Method of Slices were modified to take into consideration the unsaturated shear strength, unit weight variation in the unsaturated zone, and hydrostatic pressure changes in response to the water level fluctuation of a reservoir. Both seepage and slope analysis modules were validated against commercial programs. Analysis results obtained with the validated framework clearly revealed the distinct influences of the three factors in representative silty and sandy slopes.

Keywords Slope stability · Transient analysis · Unsaturated shear strength · Water level fluctuation

1 Introduction

Landslides are natural disasters that can cause huge property and human losses in living areas [11, 24, 27]. In recent years, climate change has altered the environment, specifically the water level of surface water bodies such as reservoirs, along with the frequency and intensity of rainfall events [22]. The water level fluctuation of surface water and rainfall infiltration influences the pore water distribution and the groundwater table in nearby slopes, which may lead to more landslides due to the shear strength reductions or deformations [12, 26].

Many case studies have identified the water level fluctuation in the reservoir as a major reason for landslides [14, 17, 20, 30, 36, 41]. The Three Gorges Dam in China is one of the well-known examples that have triggered numerous landslides in the surrounding areas due to the water level changes in the reservoir [18, 19]. Oya et al. [25] found that a rapid drawdown after flood loading could cause riverbank failures due to the reduction in the stabilizing effect of the hydrostatic pressure. Besides, the slow pore water drainage of fine-grained material was reported as another important factor for the soil strength reduction in the slopes subjected to river water level fluctuations [20].

Despite the efforts, the influence of the water drawdown velocity on the safety factor variations, especially that in different types of soils, still requires more investigation. In existing studies on water level fluctuations [6, 20, 30, 39], the shear strength of unsaturated soil in the slope stability analysis was generally described using a linear unsaturated shear strength model, i.e., the Fredlund et al. [8], or nonlinear models, i.e., the Vanapalli et al. [33] and the Fredlund et al. [9]. The linear model assumed a constant ϕ^{b} value for the unsaturated shear strength, while the

✉ Zhen Liu
zhenl@mtu.edu

Aynaz Biniyaz
abiniyaz@mtu.edu

Behnam Azmoon
bazmoon@mtu.edu

[1] Michigan Technological University, 1400 Townsend Drive, Houghton, MI 49931, USA

nonlinear models included the Soil Water Characteristic Curve (SWCC) via a unit-less volumetric water content function [40]. The influence of unsaturated soil strength models in the stability analysis of slopes during a water level fluctuation has not been thoroughly studied. In addition, rare attention has been paid to the fact that the soil unit weight changes spatially in the unsaturated zone of the slope during the transient saturated–unsaturated flow, which may considerably change the stability analysis results especially for the fine-grained materials.

To fill the above-mentioned knowledge gaps, this paper presents a framework that seamlessly couples seepage and slope stability analysis to better understand the influence of water level changes on the safety status of slopes. In particular, three factors that are possibly significant yet have not been well considered in previous studies are investigated: (1) two different unsaturated shear strength models including the Fredlund et al. [8] and the Vanapalli et al. [33], (2) soil unit weight variation due to the changes of the degree of saturation in both the time (temporal) and the computational domain of slope (spatial), and (3) the influence of the water drawdown velocity on the magnitude and pattern of factor of safety (FS) variations. It is believed that discussions on these factors need to be done with respect to soil types. Therefore, two representative types of soils (a sand and a silt) are adopted in all the analyses.

In the following sections, details for the coupled framework, including mathematical models for both seepage analysis and slope stability analysis, and the numerical implementation of the framework will be presented first. This coupled seepage and slope stability analysis framework was developed in Python to holistically (1) determine the pore water pressure distribution in the slope within the transient saturated–unsaturated flow using a Finite Element Method (FEM), and (2) analyze the stability of the slope by implementing the pore water pressure distribution at each time step using both the Bishop Simplified method (BS) and the Ordinary Method of Slices (OMS), which were modified to consider the unsaturated shear strength models, spatial variation in the soil unit weight, and hydrostatic forces of the partially submerged slope. The framework was validated against commercial software and via cross-validation to confirm the accuracy. Analyses of different scenarios were performed to consider the three factors and summarized to reach insights that deepen our understanding of this issue.

2 Method: framework for coupled seepage–stability analysis

In recent years, different frameworks have been proposed for coupling the seepage and stability analysis in partially saturated slopes [2, 6, 10, 13, 16, 20, 21, 28]. The proposed frameworks mainly employed commercial programs such as SVFLUX, SVSLOPE, SEEP/W, and SLOPE/W. Despite the fact that these packages make the modeling process easier, they are not free and easy to access for everyone. Thus, this study presents a framework written in a free and open-source programming language, Python. Another great advantage of this open-source platform is the flexibility and convenience of further modifying the governing equation and auxiliary equations for more complicated and customized seepage and stability analyses. In the proposed framework in this study, transient saturated–unsaturated seepage analysis was implemented with an open-source Python library, DOLFIN, coupled with slope stability analysis programmed with Python (ver. 3.7.2). DOLFIN is a Python interface of FEniCS which solves nonlinear Partial Differential Equations (PDEs) using the FEM. This open-source finite element analysis platform enabled the seepage analysis to model the dynamically changing boundary conditions in response to flooding and rapid water level drawdown. Seepage analysis yielded pore water pressure distributions in the slope during a water level fluctuation, which were used to analyze the stability of the slope at each time-step. The slope stability was analyzed with two Limit Equilibrium Methods (LEMs), i.e., the BS and the OMS, which were modified to allow for the variation in the degree of saturation and the subsequent varying unit weight of soil, unsaturated shear strength models, and the changes in the hydrostatic pressure.

2.1 Seepage analysis: mathematical model

2.1.1 Governing equation for the transient saturated–unsaturated flow

The governing equation for a transient saturated–unsaturated model was obtained by modifying the Richards equation [23],

$$S\frac{\partial(h+z)}{\partial t} = K \times \nabla(\nabla(h+z)), \qquad (1)$$

where S and K were defined based on the degree of saturation (Eq. 2):

$$\begin{cases} \text{Saturated Flow} \rightarrow K = K_s, \; S = S_s \\ \text{Unsaturated Flow} \rightarrow K = K_s K_r, \; S = S_c \end{cases}, \qquad (2)$$

where h[m] is the pressure head, z[m] is the elevation head,

t is time, $K[m/s]$ is the hydraulic conductivity, $S_s[1/m]$ is the specific storage of saturated flow, and $S_c[1/m]$ is the specific moisture capacity for unsaturated flow. In saturated flow, the saturated hydraulic conductivity, K_s, was used in the equation; for unsaturated flow, K was replaced with $K_s K_r$, where $K_r[-]$ is the relative hydraulic conductivity. K_r defines how the hydraulic conductivity changes with the effective degree of saturation (S_e). One widely adopted relationship for K_r proposed by van Genuchten [32] was used:

$$k_r = S_e^b \left(1 - \left(1 - S_e^{1/a}\right)^a\right)^2, \tag{3}$$

where a and b are empirical parameters and S_e is the effective degree of saturation. The hydraulic conductivity decreases as the effective degree of saturation decreases.

The effective degree of saturation, S_e, is related to the suction via the SWCC. In this study, an equation provided by van Genuchten [32] was adopted:

$$S_e = \frac{S_w - S_r}{1 - S_r} = \left[1 + \left(\frac{\psi}{P_0}\right)^{\frac{1}{1-a}}\right]^{-a} \tag{4}$$

where $S_w[-]$ is the water saturation, $S_r[-]$ is the residual saturation, $\psi[Pa]$ is the matric suction, and P_0 [Pa] is a parameter related to the air entry value (AEV) [3, 40].

To close the equation system, Eq. 4 is rewritten in terms of water head (h) as Eq. 5:

$$S_e = \left[1 + \left(\frac{\gamma_w h}{P_0}\right)^{\frac{1}{1-a}}\right]^{-a} = \left[1 + \left(\frac{9810 \times |h|}{P_0}\right)^{\frac{1}{1-a}}\right]^{-a}, \tag{5}$$

where $\gamma_w[N/m^3]$ is the unit weight of water and $h[m]$ is the negative pore-water head representing the matric suction.

The specific storage for the saturated flow, $S_s[1/m]$, is the volume of water released from a unit volume of aquifer per unit decline in the hydraulic head. S_s is the function of the compressibility of soil and water and the soil porosity [29]:

$$S_s = \frac{1}{V_t}\frac{dV_w}{dh} = \gamma_w(C_s + n C_w), \tag{6}$$

where $C_s[ms^2/kg]$ is the soil compressibility, $n[-]$ is the soil porosity, and $C_w[ms^2/kg]$ is the water compressibility.

The specific moisture capacity for unsaturated flow, $S_c[1/m]$, defines the rate of change in the water content per unit change of the negative water head. S_c is a function of h, which can be obtained using Eq. 7:

$$S_c = \left|\frac{\partial \theta}{\partial h}\right| = n\frac{\partial S_e}{\partial h}, \tag{7}$$

where $\theta[-]$ is the volumetric water content.

2.2 Materials

In this study, two representative soils, i.e., a sand and a silt, were chosen to assess the influence of soil types. Material properties for the transient saturated–unsaturated flow model for the sand and silt were adopted from a published study [3] (see Table 1). Figure 1 presents the SWCC and the relationship between the relative hydraulic conductivity and the effective saturation for the chosen silty and sandy soils. Empirical parameters including a, b, and P_0 were derived from SWCC reported in Cho [3]. It is noted that the values of the specific storage (S_s) for saturated flow were assumed based on the ranges provided by Sethi and Di Molfetta [29] for sands and silts.

2.2.1 Geometry and boundary conditions

A typical water level fluctuation profile, illustrated in Fig. 2, was adopted in this study. First, the water level in the reservoir rises from 9 to 15 m in 35 days with a constant velocity of $V_r = 0.171$ m/day. Then, the water level remains constant for 15 days. In the following 20 days, the water level decreases with a higher velocity of $V_d = 0.3$ m/day. Eventually, the water level in the reservoir stays at 9 m for 20 days. Modifications to this profile were made for sensitivity analysis of the water level drawdown velocity on the FS. More details are given in Sect. 4.4.

Figure 3 shows the geometry and boundary conditions for the slope next to the reservoir. As shown, the boundary condition on the right side of the slope was set to a constant total water head of 9 m, while the boundary condition of the left side was a water head changing with time as the water level in the reservoir fluctuates. The initial level of water in the slope was 9 m before the water level fluctuation.

Dirichlet and Neumann boundary conditions were used to formulate the constant hydraulic head and flux, respectively. The bottom boundaries, i.e., "FE," and "PC" and "CD" were set to "no flux" and were mathematically formulated as Eq. 8:

$$-\nabla(h + z) \cdot \vec{n} = 0 \text{ on } \Gamma_{(FE, PC, CD)} \text{ for } t > 0, \tag{8}$$
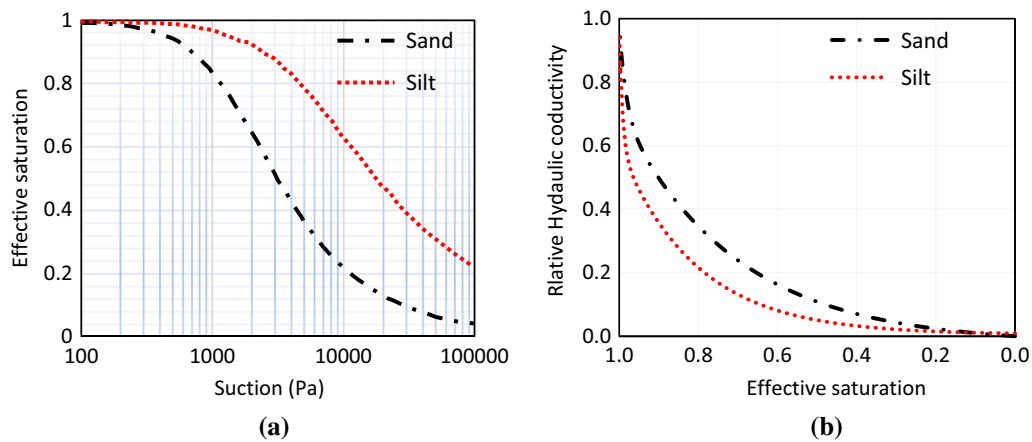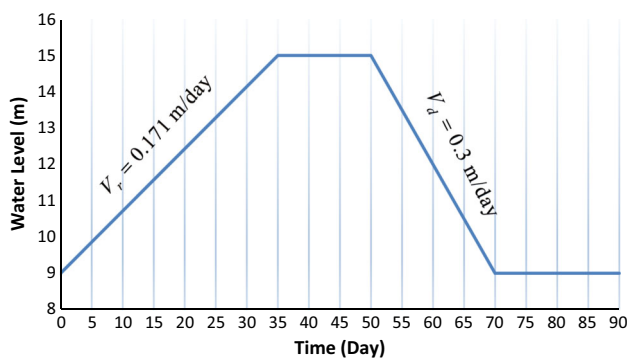
"DE" was set to a Dirichlet boundary condition that represents a constant water head as Eq. 9:

$$h + z = 9 \text{ on } \Gamma_{(DE)} \text{ for } t > 0, \tag{9}$$

The remaining boundaries "FA," "AB," and "BP" were set to a special dynamic Dirichlet boundary condition as below, which represents the water level fluctuation in the neighboring water reservoir:
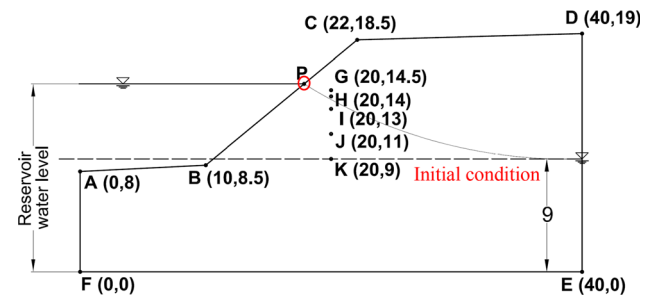
Table 1 Material properties for the seepage model adopted from Cho [3] and Sethi and Di Molfetta [29]

Model input	Definition	Sand	Silt
K_s	Saturated hydraulic conductivity (m/s)	1×10^{-5}	3×10^{-6}
S_r	Residual saturation	0	0
S_s	Saturated specific storage (1/m)	1×10^{-4}	1×10^{-3}
a	Empirical parameter	0.445	0.336
b	Empirical parameter	0.5	0.5
P_0	Empirical parameter (Pa)	1500	4905
n	Porosity	0.35	0.5

Fig. 1 Properties of two representative soils documented in Cho [3]: **a** SWCC and **b** relative hydraulic conductivity (k_r) vs. effective degree of saturation (S_e)

Fig. 2 Typical fluctuation of the reservoir water level in 90 days

Fig. 3 Cross section of the slope subjected to the reservoir water fluctuation (unit: m)

$$\begin{array}{ll} h + z = 9 + 0.171t & \text{if } 0 \text{ days} < t < 35 \text{ days} \\ h + z = 15 & \text{if } 35 \text{ days} < t < 50 \text{ days} \\ h + z = 15 - 0.3(t - 50) & \text{if } 50 \text{ days} < t < 70 \text{ days} \\ h + z = 9 & \text{if } 70 \text{ days} < t < 90 \text{ days} \end{array} \tag{10}$$

To implement the dynamic boundary condition for "BC," the point "P" was defined as a variable changing with time. At each time step, the coordinate of "P" was updated as follows

$$y_p = \begin{cases} 9 + 0.171t & \text{if } 0 \text{ days} < t < 35 \text{ days} \\ 15 & \text{if } 35 \text{ days} < t < 50 \text{ days} \\ 15 - 0.3t & \text{if } 50 \text{ days} < t < 70 \text{ days} \\ 9 & \text{if } 70 \text{ days} < t < 90 \text{ days} \end{cases}, \tag{11}$$

$$x_p = x_B + \frac{x_C - x_B}{y_C - y_B}(y_p - y_B) \tag{12}$$

Additionally, it is required to set an initial value for the total head of the system, i.e., 9 m, as the initial condition to solve the governing equation,

$$h + z = 9 \quad \text{in } \Omega \text{ at } t = 0, \tag{13}$$

2.3 Slope Stability Analysis: Mathematical Model

For the slope stability analysis using LEMs, the BS [1] and the OMS [7] were selected considering their wide acceptance and convenience in automating the computational process. However, modifications are needed for the *FS* equations in the conventional BS and OMS to allow slope stability analysis to be integrated with a transient saturated–unsaturated flow. These modifications include (1) spatial variation in the soil unit weight, (2) unsaturated shear strength models, and (3) hydrostatic forces induced by a water level fluctuation.

Figure 4 shows a schematic of the stability analysis for a partially submerged slope. As shown in Fig. 4a, slip surfaces in the stability analysis were searched using the "grid-radius" method. In this method, a range was defined for the center coordinate (X_c, Y_c) and the radius (R) of circular slip surfaces, and then, trial slip surfaces were generated by various combinations of X_c, Y_c, and R. It is a common practice that, in both the BS and OMS, the soil body above the circular slip surface is divided into a given number of vertical slices (N_x). In addition to the vertical slices, in this study, each vertical slice was also divided into a given number of cells (N_c) to more accurately consider the soil mass above the slip surface. Figure 4b shows the forces and stresses acting on a typical vertical slice. In this figure, F_w is the hydrostatic force induced by the water in the reservoir, W is the total weight of the vertical slice, τ is the mobilized shear stress at the base of the vertical slice, and σ_n is the total normal stress on the base of the vertical slice. In the following subsections, the required
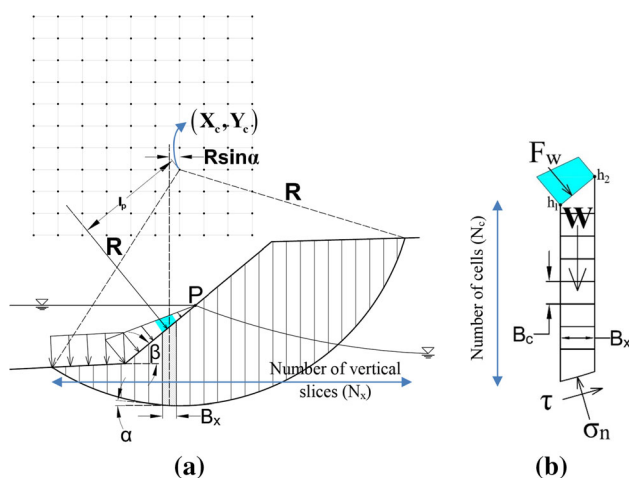

Fig. 4 Illustration of the stability analysis for the partially submerged unsaturated slope: **a** "grid-radius" method to search trial slip surfaces and **b** forces and stresses acting on a vertical slice

modifications for the computations of the BS and OMS will be discussed.

2.4 Spatial variation in the soil unit weight

In conventional slope stability analysis using LEMs, the dry unit weight and saturated unit weight are usually used for the unsaturated and saturated zones in the slope, respectively. The assumption of the dry unit weight for the unsaturated zone may underestimate the driving forces of the slip surface. This is because the soil unit weight changes as the degree of saturation changes spatially and temporally during the water level fluctuation. This relationship was formulated as Eq. 14, which can be derived from relationships between basic soil index properties [4],:

$$\gamma = \frac{G_s + S_e e}{1 + e} \gamma_w = \gamma_{dry} + n S_e \gamma_w, \tag{14}$$

where $\gamma[\text{kN}/\text{m}^3]$ is the natural unit weight of the soil, $G_s[-]$ is the specific gravity of soil particles, $e[-]$ is the void ratio, $n[-]$ is the porosity, $\gamma_{dry}[\text{kN}/\text{m}^3]$ is the dry density of soil, $\gamma_w[\text{kN}/\text{m}^3]$ is the unit weight of water, and $S_e[-]$ is the effective saturation of the soil. The first step to more accurately calculate the weight of the soil mass above the slip surface was to divide the slip surface into vertical slices, and the slices were then evenly divided into cells. Next, for each cell, the degree of saturation was calculated with Eq. 5 using the pore water head distribution results from the seepage analysis. Then, the unit weight of the soil was calculated using Eq. 14. Eventually, the weight of a vertical slice j, W_j, was computed using Eq. 15:

$$W_j = \sum_{k=1}^{N_c} B_x B_c \gamma_k, \tag{15}$$

where $B_x[\text{m}]$ is the width of the vertical slice j, $B_c[\text{m}]$ is the height of the cells within the vertical slice j, γ_k is the soil unit weight of the cell k within the vertical slice j, and N_c is the number of cells within individual vertical slices.

2.4.1 Unsaturated shear strength

In this study, two common models for the unsaturated shear strength, i.e., the Fredlund et al. [8] (Eq. 16) and the Vanapalli et al. [33] (Eq. 17), were considered to assess the influence of such models on the slope stability analysis of variably saturated slopes with an emphasis on the water level fluctuation. Both models were also used to investigate the influence of the effective saturation on the results of *FS*:

$$\tau = c' + (\sigma_n - U_a) \tan \phi' + (U_a - U_w) \tan \phi^b, \tag{16}$$

$$\tau = c' + (\sigma_n - U_a) \tan \phi' + (U_a - U_w)[\tan \phi' S_e], \tag{17}$$

where $\tau[\mathrm{kN/m^2}]$ is the shear strength of the unsaturated soil, $c'[\mathrm{kN/m^2}]$ is the effective cohesion, $\phi'[°]$ is the effective internal friction angle, $\sigma_n[\mathrm{kN/m^2}]$ is the total normal stress, $\phi^b[°]$ is the angle representing the rate of increase in the shear strength relative to the matric suction, S_e is the effective degree of saturation, and $U_a - U_w[\mathrm{kN/m^2}]$ is the matric suction in which U_a is the pore air pressure and U_w is the pore water pressure. This study ignores changes in the pore air pressure considering that its influence in seepage processes without high flow speeds and pressures is negligible [31]. To determine $U_w = \gamma_w h$ for a vertical slice, the pore water head (h) at the base of the vertical slice was derived from the pore water head distribution resulting from the seepage analysis.

2.4.2 Hydrostatic forces

In a partially submerged slope, the hydrostatic forces may play a significant role in the stability of the slope [37]. Thus, it is required to modify the BS and OMS to consider the effects of hydrostatic forces. In this study, the pore water head on the top of each vertical slice (see Fig. 4b), i.e., h_1 and h_2, was derived from the pore water head distribution from the seepage analysis. Positive values of h_1 and h_2 indicate that the vertical slice is submerged, while negative values mean that there is no water on the top of the selected vertical slice. For the submerged vertical slice, the hydrostatic force, F_w, was calculated with Eq. 18:

$$F_w = \gamma_w \left(\frac{h_1 + h_2}{2}\right)\left(\frac{B_x}{\cos \beta}\right), \tag{18}$$

where β is the angle between the slope surface and the horizontal direction.

2.4.3 Modified BS

The BS was modified to consider unsaturated shear strength models, spatial variation in the soil unit weight, and hydrostatic forces. The FS of the original BS was obtained as Eq. 19:

$$FS = \frac{\sum_{j=1}^{N_x} \frac{1}{m_a}\left[c' + \left(\frac{W_j}{B_x} - U_{w_j}\right)\tan \phi'\right]}{\sum_{j=1}^{N_x} \frac{W_j}{B_x}\sin \alpha_j} \tag{19}$$

where W_j is the total weight of the vertical slice j, U_{w_j} is the pore water pressure at the mid-point of the base of the vertical slice j, and m_a is defined as.

$$m_a = \cos \alpha_j + \frac{1}{FS}\sin \alpha_j \tan \phi', \tag{20}$$

where α_j is the angle between the tangent to the base of the vertical slice j and the horizontal direction.

The FS equation was derived by ensuring (1) the force equilibrium in the vertical direction to determine the total normal stress (σ_n) for a typical vertical slice and (2) the moment equilibrium about the center of the slip surface to determine the FS. The inter-slice side forces were neglected because they do not make a noticeable difference in the results [15]. From the force equilibrium for the vertical slice j, σ_{nj} was derived as Eq. 21,

$$\sigma_{n_j} = \frac{W_j}{B_x} + F_{w_j}\cos \beta - \tau_j \tan \alpha_j, \tag{21}$$

where τ_j is defined with Eq. 22 for BS considering the Fredlund et al. [8] model for the unsaturated shear strength:

$$\tau_j = \frac{1}{FS}\left[c' + (\sigma_n - U_a)_j\tan \phi' + (U_a - U_w)_j\tan \phi^b\right], \tag{22}$$

σ_n is obtained by replacing τ_j in Eq. 21 with Eq. 22. Finally, the FS was derived via the consideration of the moment equilibrium about the center of the slip surface, see Eq. 23:

$$FS = \sum_{j=1}^{N_x} \frac{1}{m_a m_b} \left[c' + \left(m_c - U_{a_j}\right)\tan \phi' + (U_a - U_w)_j\tan \phi^b\right], \tag{23}$$

where $(U_a - U_w)_j$ is the matric suction at the mid-point of the base of the vertical slice j, and m_b and m_c are defined as:

$$m_b = \frac{W_j \sin \alpha_j}{B_x} - \frac{(F_w l_p)_j}{RB_x}, \tag{24}$$

$$m_c = \frac{(W_j + F_{w_j}\cos \beta)}{B_x}, \tag{25}$$

where l_p is the moment arm of F_w about the center of the slip surface (see Fig. 4a).

Equation 26 is the modified FS equation with the Vanapalli et al. [33] model

$$FS = \sum_{j=1}^{N_x} \frac{1}{m_a m_b} \left[c' + \left(m_c - U_{a_j}\right)\tan \phi' + (U_a - U_w)_j\tan \phi' S_{e_j}\right], \tag{26}$$

where S_{ej} is the effective saturation at the mid-point of the base of the vertical slice j. Iterations are needed for calculating the safety factor through BS because FS" appears on both sides of the equation.

2.4.4 Modified OMS

The OMS developed by Fellenius [7] is another common LEM. Whitman and Moore [38] demonstrated that the values of *FS* predicted with the OMS were usually lower than the true values. Despite such findings, the OMS was still implemented to cross-validate BS. Equation 27 is the *FS* equation of the conventional OMS:

$$FS = \sum_{j=1}^{N_x} \frac{B_x}{W_j \sin^2 \alpha_j} \left[c' + \left(\frac{W_j}{B_x} \sin \alpha_j \cos \alpha_j - U_{w_j} \right) \tan \phi' \right],$$
(27)

This method ensures the force equilibrium in the direction normal to the arc at the mid-point of the base for every vertical slice to determine the total normal stress (σ_n). It is noted that this direction changes between vertical slices. Then, the *FS* is calculated via the consideration of the moment equilibrium about the center of the slip surface. The OMS neglects both inter-slice normal and shear forces. The simplicity of the *FS* calculation is a major advantage of this method, while the major disadvantage is the slightly lower accuracy compared with the BS. Considering the force equilibrium for the vertical slice *j*, σ_{nj} was derived as follows:

$$\sigma_{n_j} = \frac{\cos^2 \alpha_j}{B_x} \left[W_j + F_{w_j} \cos \beta \right],$$
(28)

The *FS* was then derived from the moment equilibrium as Eq. 29,

$$FS = \frac{\sum_{j=1}^{N_x} \tau_j B_x \sec \alpha_j R}{\sum_{j=1}^{N_x} \left[W_j \sin \alpha_j R - \left(F_w l_p \right)_j \right]},$$
(29)

where τ_j is defined using Eq. 30 based on the Fredlund et al. [8] model for the unsaturated shear strength as:

$$\tau_j = c' + (\sigma_n - U_a)_j \tan \phi' + (U_a - U_w)_j \tan \phi^b,$$
(30)

By replacing τ_j in Eq. 29 with Eq. 30, the *FS* equation modified with the Fredlund et al. [8] model was obtained as Eq. 31:

$$FS = \sum_{j=1}^{N_x} \frac{1}{\cos \alpha_j m_b}$$
$$\left[c' + \left(m_c \cos^2 \alpha_j - U_{a_j} \right) \tan \phi' + (U_a - U_w)_j \tan \phi^b \right],$$
(31)

Equation 32 is the modified *FS* equation with the Vanapalli et al. [33] model for the unsaturated shear strength:

$$FS = \sum_{j=1}^{N_x} \frac{1}{\cos \alpha_j m_b}$$
$$\left[c' + \left(m_c \cos^2 \alpha_j - U_{a_j} \right) \tan \phi' + (U_a - U_w)_j \tan \phi' S_{e_j} \right],$$
(32)

Model parameters for the slope stability analysis are provided in Table 2. It is noted that the value of ϕ^b was assumed to be $\phi'/2$ for both the sand and silt [12, 34].

2.5 Numerical implementation

The above framework was implemented using Python code to automatically search for the minimum *FS* of the partially submerged and unsaturated slope during the water level fluctuation. A detailed procedure for implementing the coupled transient seepage and slope stability analysis is illustrated in the flowchart shown in Fig. 5.

The flowchart was organized around two major goals: (1) finding the pore water head distribution obtained from the transient seepage analysis and (2) analyzing the stability of the slope during the transient flow. To achieve the first goal, the DOLFIN package, which is a Python interface of a finite element analysis platform, FEniCS, was utilized. The governing equation for the transient saturated–unsaturated flow is a time-dependent PDE, which was solved by implementing the FEM-variational formulation. The solution of the PDE is the total head ($h + z$), which varies in both time and space. Input parameters for the transient seepage analysis include unsaturated soil characteristics (a, b, P_0, u_a), saturated specific storage (S_s), saturated hydraulic conductivity (K_s), slope geometry, boundary conditions, initial water table, and time variables (total time of the water level fluctuation, $T = 90$ days, and the number of time steps to for calculating the time step, $\Delta t = T/num\_steps$).

To solve the PDE using the FEM, a mesh consisting of 3-node Lagrangian elements was generated in the computational domain of the slope (Ω). Neumann and Dirichlet boundary conditions were assigned to the defined subdomains as described in Sect. 2.1.3. The initial boundary condition was specified as the solution to the PDE at t = 0. Auxiliary equations for the unsaturated hydraulic conductivity and effective saturation were given to the model. Next, the PDE for the governing equation was reformulated as a finite element variational problem. For each time-step, the boundary conditions were updated based on the water level at a time t_i as described in Sect. 2.1.3. Solving the PDE yielded the total water head distribution at the time t_i. Subtracting the elevation head from the total water head surrendered the pore water head distribution which was later employed in the stability analysis.

Table 2 Model parameters for slope stability analysis

Model input	Definition	Sand	Silt
γ_{dry}	Dry unit weight of soil (kN/m^3)	16.40	16.40
γ_{sat}	Saturated unit weight of soil (kN/m^3)	19.83	21.30
ϕ'	Friction angle	35°	30°
c'	Cohesion (kN/m^2)	3	10
ϕ^b	The angle representing the rate of increase in the shear strength relative to the matric suction	17.5°	15°
U_a	Pore air pressure	0	0
N_x	Number of vertical slices	100	100
N_c	Number of cells within the vertical slices	20	20

The inputs for the stability analysis at the time t_i are relevant soil parameters (C', ϕ', γ_{dry}, n, a, P_0, ϕ^b), the numbers of vertical slices (N_X), the number of cells within the vertical slices (N_C), the slope geometry, and the water head distribution at the time t_i. Trial slip surfaces were generated using the defined range of the center coordinates (X_c, Y_c) and the radius (R). Each trial slip surface was divided into N_X vertical slices. The shear force at the midpoint of the base and the hydrostatic force at the top were calculated for the submerged vertical slice. However, for the unsubmerged vertical slice, only the shear force was calculated. The vertical slice j was then divided into N_C cells. To compute the accurate weight of each cell, the degree of saturation was first calculated at the center of the cell using the pore water head distribution. It is worthwhile to mention that the pore water head of the closest node to the center of the cell was adopted to proceed with the calculations. The computation process ends when the weight of the trial slip surfaces is obtained. Next, the *FS* for the trial slip surfaces was calculated using the modified BS and OMS. The coupled seepage and slope stability analysis was repeated for the time t_{i+1} until $t_{i+1} > 90$ days. It is worth noting that the slope stability analysis was limited to specific times during the water level fluctuation due to the high computational cost of the slope stability analysis. In the end, the minimum *FS* was obtained for the desired times during the water level fluctuation.

3 Validation

The computer code for the coupled transient seepage and slope stability analysis was validated for both the transient seepage analysis and slope stability analysis. To validate the written code for the seepage analysis, another finite element PDE solver, FlexPDE Ver. 6.36 s, was used. The Python script for the slope stability analysis was validated using GeoStudio SLOPE/W Ver. 2020, a widely adopted

slope stability program. It is worthwhile to mention that the developed code is needed despite the existence of programs like FlexPDE and GeoStudio because such programs cannot be seamlessly implemented with the aforementioned modifications, which are required for this study.
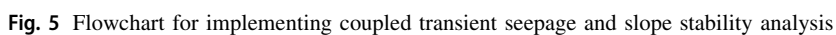
3.1 Validation of transient seepage analysis

The newly developed code for transient seepage analysis was validated against a general-purpose scripted finite element model builder to solve first or second-order PDEs, FlexPDE [23]. This commercial package has been widely adopted for solving PDEs due to its easy implementation. However, modeling the complex boundary conditions such as flooding and drawdown cannot be easily implemented in FlexPDE. Thus, for the validation, a transient flow case that includes an alternative quasi-static boundary condition for a sudden water level change was simulated with both the new code and FlexPDE. This consideration is adequate to validate the mathematical system of the seepage model in this study.

In this case, the numerical model was defined with the same geometry (see Fig. 3), initial condition (Eq. 13), and the silty soil properties (Table 1) as described in previous sections. The duration of the transient flow was 35 days. The boundaries "FA," "AB," and "BP" were defined as constant Dirichlet boundary conditions representing a constant water level of the reservoir, i.e., 15 m:

Dirichlet BC

$$h + z = 15 \quad \text{on } \Gamma_{(AF, AB, BP)}, \tag{33}$$

The remaining boundaries are similar to those in the model introduced in Sect. 2.1.3. To validate the results, two different paths were defined: (1) from (0, 0) to (40, 19) (2) from (10.6, 9) to (40, 9). This difference between the water level of the reservoir, which is exhibited as the difference between the water head on "BC" and the initial groundwater table, would trigger seepage that is similar to what happens in a slope after a water drawdown.

Fig. 5 Flowchart for implementing coupled transient seepage and slope stability analysis
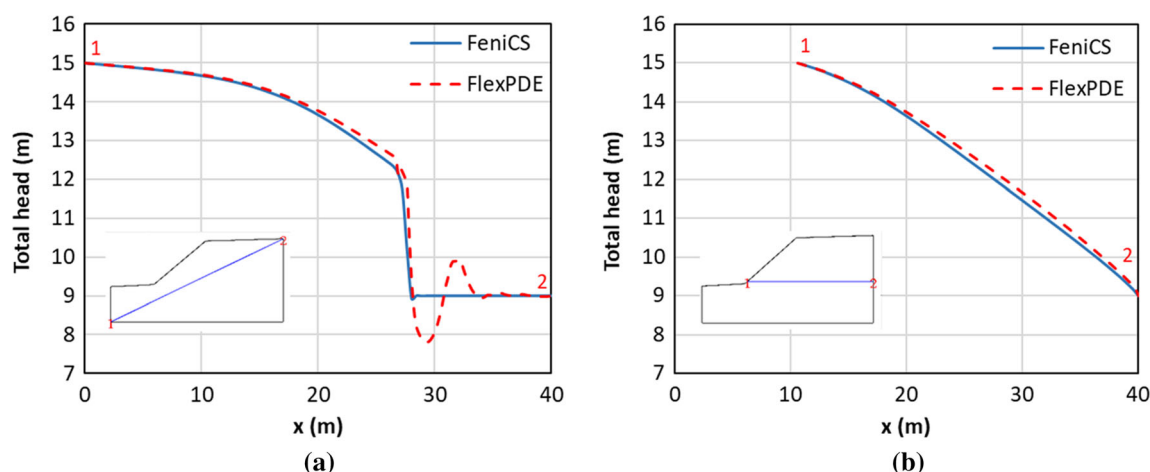
Fig. 6 Validation of transient saturated–unsaturated seepage model in FeniCS against FlexPDE for silty slope at t = 35 days along **a** path plot from (0, 0) to (40, 19) and **b** path plot from (10.6, 9) to (40, 9)

The solutions of the seepage analysis from the written code and FlexPDE, i.e., the total water head (h + z or u), were compared along the two paths in the slope as shown in Fig. 6. A comparison of the path plots from FEniCS and FlexPDE shows that the results from FlexPDE closely agree with the results from FEniCS. In Fig. 6a, there is a noticeable oscillation in the FlexPDE result, where the saturated soil meets the unsaturated soil. This is because the PDE is highly nonlinear at the boundary of saturated and unsaturated zones. It is also noted that there is a negligible oscillation in the FeniCS result at the same location. In fact, the smaller oscillation in the FeniCS result compared to the FlexPDE result in Fig. 6a indicates that the seepage analysis implemented in this study with FEniCS with a more delicate temporal difference scheme is more reliable than FlexPDE for the targeted transient saturated–unsaturated seepage analysis.

3.2 Validation of slope stability analysis

The written Python script for the slope stability analysis in this study was validated using SLOPE/W. SLOPE/W was selected because it provides an advanced option to consider the unit weight variation in the unsaturated zone via a user-defined volumetric water content function. By contrast, other common slope stability programs such as SVSLOPE and Slide2 can only consider one average value for the unsaturated soil unit weight above the water table.

The stability analysis was validated for both sandy and silty slopes using the modified BS and OMS with the Vanapalli et al. [33] model for the unsaturated shear strength. For simplicity, the FS values were only validated for the initial level of the groundwater table at t = 0, i.e., 9 m (see Fig. 3). Soil properties for the sandy and silty slopes are listed in Table 2.

Table 3 Comparison of FS values from SLOPE/W and the proposed computer code

Type of soil	Limit equilibrium method	New code	SLOPE/W
Sand	BS	1.301	1.301
	OMS	1.246	1.239
Silt	BS	1.633	1.636
	OMS	1.556	1.543

Calculated FS values using the modified BS and OMS in this study (new code) and SLOPE/W are listed in Table 3 for the defined silty and sandy slopes. The results from SLOPE/W confirmed the accuracy of the Python code in this study.

4 Results and discussions

4.1 *FS* variation in typical water level fluctuation processes

Figure 7a and b shows the results of the stability analysis for the silty and sandy slopes during the 90 days of water level fluctuation, respectively. These figures also provide a comparison between the modified BS and OMS with the Vanapalli et al. [33] model for the unsaturated soil shear strength. For the silty slope, it was observed that the modified BS yielded FS results that are 3.8% to 17.0% greater than the FS results obtained from the modified OMS. For the sandy slope, the FS results calculated with the modified BS are 4.5% to 9.1% greater than those computed using the modified OMS. It was noticed that the two selected methods do not necessarily lead to the same
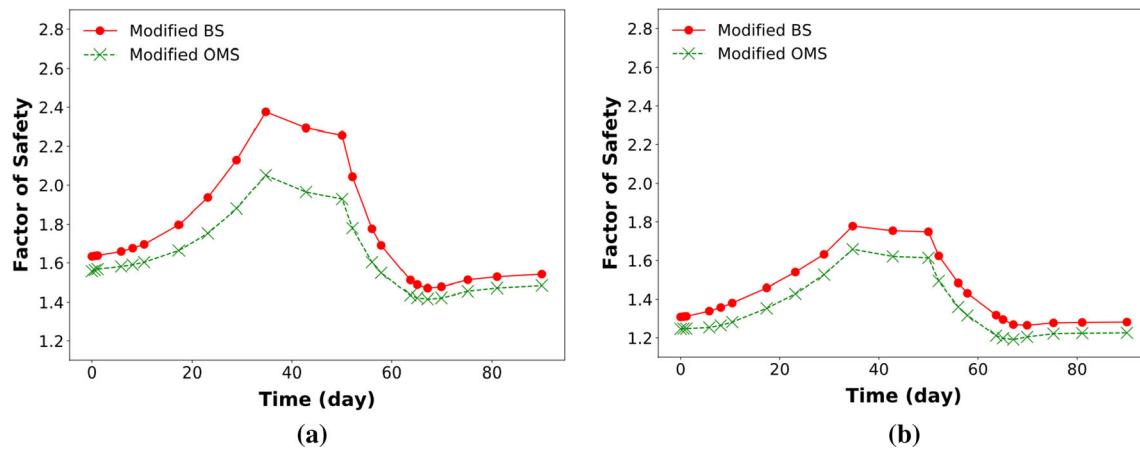
Fig. 7 *FS* variation during water level fluctuation using two modified LEM methods with Vanapalli et al. [33] model in **a** silty slope and **b** sandy slope

critical slip surface in the condition of identical materials, geometry, and boundary conditions.

Despite the difference between BS and OMS results reported above, the modified BS was selected to conduct the *FS* analysis hereafter considering that the BS is more widely adopted for its reliable performance in most cases [5, 35].

When the reservoir water level increases, i.e., $t = 0 - 35$ days, Fig. 7a and b shows that the *FS* increases as the hydrostatic pressure induced by the reservoir water level increases. By rising the reservoir water level from 9 to 15 m, the *FS* of the silty slope experiences a 45.4% increase, i.e., from 1.63 to 2.37, and the *FS* of the sandy slope increases by 36.9%, i.e., from 1.30 to 1.78. The increase in the *FS* of the silty slope is 8.5% greater than the sandy slope. A comparison of the water tables at $t = 35$ days in silty and sandy slopes, as shown in Fig. 8a and b, helps explain this difference. The groundwater table in the sandy slope reaches a higher level than in the

silty slope under a similar condition for the reservoir water level due to the greater hydraulic conductivity of the sandy slope. A higher level of the groundwater table increases the slope's total weight, leading to a slower growth rate for the *FS*.

When the reservoir water level stays unchanged, i.e., $t = 35 - 50$ days, there is a reduction in the *FS* in both the silty and sandy slopes as shown in Fig. 7a and b, respectively. During this period, the *FS* of the silty slope decreases by 5.1%, i.e., from 2.37 to 2.25, and the *FS* of the sandy slope decreases by 1.7%, i.e., from 1.78 to 1.75. The difference in the *FS* reduction is caused by the fact that, as shown in Fig. 8a and b, the increase in the groundwater table in the sandy slope is less than the increase in the silty slope. Both cases reach the same level of groundwater table at $t = 50$ days.

During the period of water drawdown, i.e., $t = 50 - 70$ days, the hydrostatic pressure, which helps stabilize the slope as can be seen in Eq. 26, decreases
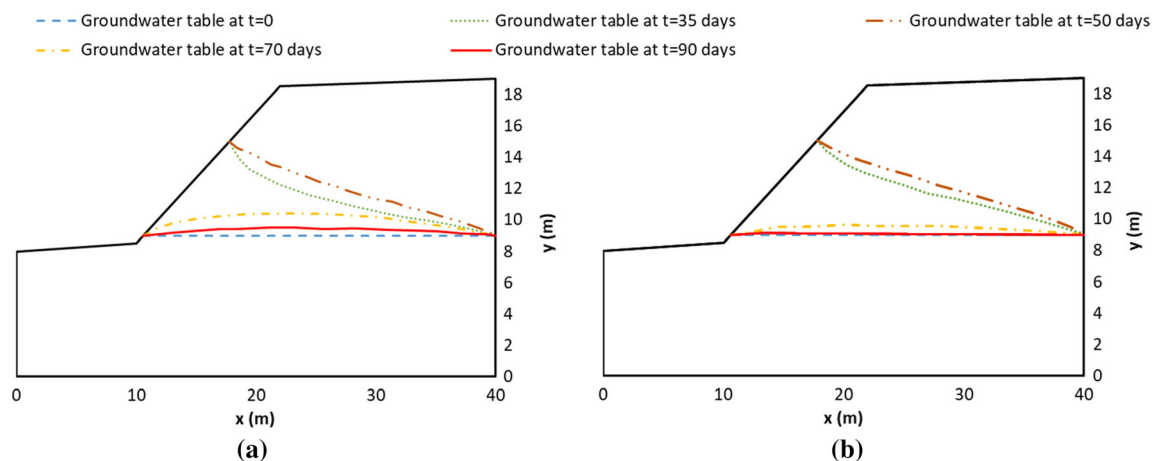

Fig. 8 Groundwater table during water level fluctuation in **a** silty slope and **b** sandy slope

continuously. As a result, the FS begins to decrease in both silty and sandy slopes. In the process, the FS of the silty slope decreases by 34.7%, i.e., from 2.25 to 1.47, and the FS of the sandy slope decreases by 28%, i.e., from 1.75 to 1.26. Observation of results revealed that the rate of decrease in the FS depends on both the velocity of water drawdown and the hydraulic conductivity. The influence of the water drawdown velocity on the FS is discussed in Sect. 4.4. A comparison of the groundwater tables at t = 70 days in Fig. 8a and b illustrates the influence of different hydraulic conductivities on the groundwater table. For a constant drawdown velocity, the rate of decrease in the FS of the silty slope with smaller hydraulic conductivity, i.e., $K_s = 3 \times 10^{-6} \frac{m}{S}$, is greater than the FS of the sandy slope. This is because a greater hydraulic conductivity in the sandy slope, i.e., $K_s = 1 \times 10^{-5} \frac{m}{S}$, expedites the drainage process and helps reduce the total weight of the slope.

After the water drawdown, i.e., $t = 70 - 90$ days, there is a slight increase in the FS in both the silty and sandy slopes. The FS of the silty slope increases by 4.8%, i.e., from 1.47 to 1.54, and the FS of the sandy slope increases by 1.6%, i.e., from 1.26 to 1.28. The decline in the groundwater table from $t = 70$ days to $t = 90$ days, as shown in Fig. 8, reduces the slope's total weight and consequently increases the FS after the water drawdown.

4.2 Influence of soil unit weight variation on FS

Figure 9 shows the influence of the soil unit weight variation on the FS in both silty and sandy slopes during the water level fluctuation. The FS results in Fig. 9a and b were calculated using the modified BS with the Vanapalli et al. [33] model with two representative assumptions of the soil unit weight in the unsaturated zone: varying soil

unit weight and constant soil unit weight (usually dry unit weight). It is noted that the saturated unit weight was assigned to the saturated zone under the groundwater table. For the sandy soil, the unit weight of the unsaturated zone varies between $\gamma_{dry} = 16.40 \, \text{kN}/\text{m}^3$ and $\gamma_{sat} = 19.83 \, \text{kN}/\text{m}^3$ based on the degree of saturation. This range for the silty soil is from $\gamma_{dry} = 16.40 \, \text{kN}/\text{m}^3$ to $\gamma_{sat} = 21.30 \, \text{kN}/\text{m}^3$. The dry soil unit weight for both the silty soil and the sandy soil is $16.40 \, \text{KN}/\text{m}^3$.

In the silty slope, as shown in Fig. 9a, the consideration of the soil unit weight variation for the unsaturated zone yielded lower values of FS compared with the curve obtained with the adoption of the dry unit weight in the unsaturated zone. This is because the consideration of the unit weight variation in the unsaturated silty soil above the water table, which better reflects the reality, increases the driving forces of landslides, i.e., the weight of the soil, and thus decreases the FS of the slope. The difference between the two curves varies from 3 to 6% during the transient flow process. By contrast, the consideration of the soil unit weight variation in the sandy slope, as shown in Fig. 9b, does not make a noticeable difference in the FS results. This contrast indicates that the influence of the unit weight variation on the FS of slopes is sensitive to the soil types. The influence of the spatial unit weight variation on FS results during the water level fluctuation can be even more significant for finer materials such as clay. On the contrary, the soil unit weight variation in the unsaturated zone of coarse-grained materials, e.g., sand and gravel, could be negligible; thus, it is safe to use the dry unit weight in the stability analysis of slopes composed of such soils.

To gain more insights into the cause of the difference, spatial distributions of the degree of saturation in silty and sandy slopes were extracted from the water head distribution. Figures 10 and 11 show the distributions at $t = 0$ and
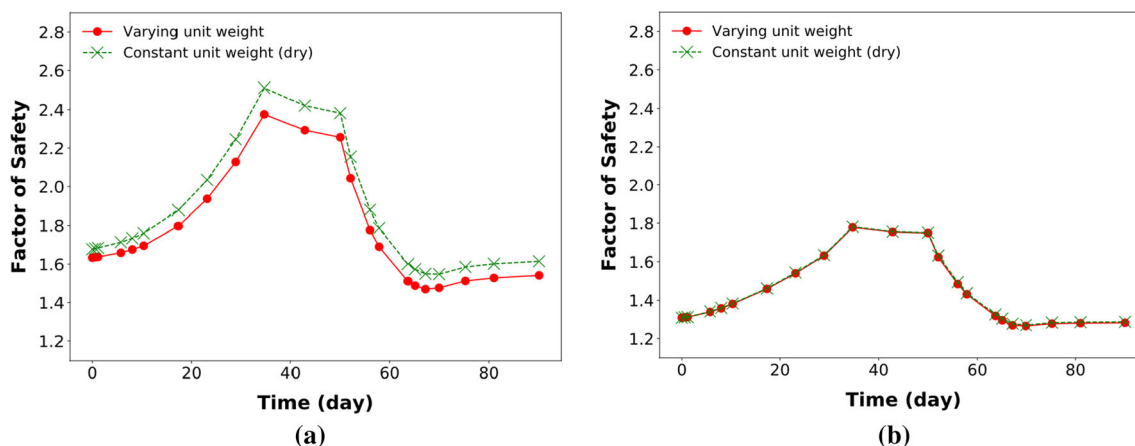

Fig. 9 Influence of soil unit weight variation on FS results obtained from modified BS with Vanapalli et al. [33] model in **a** silty slope and **b** sandy slope
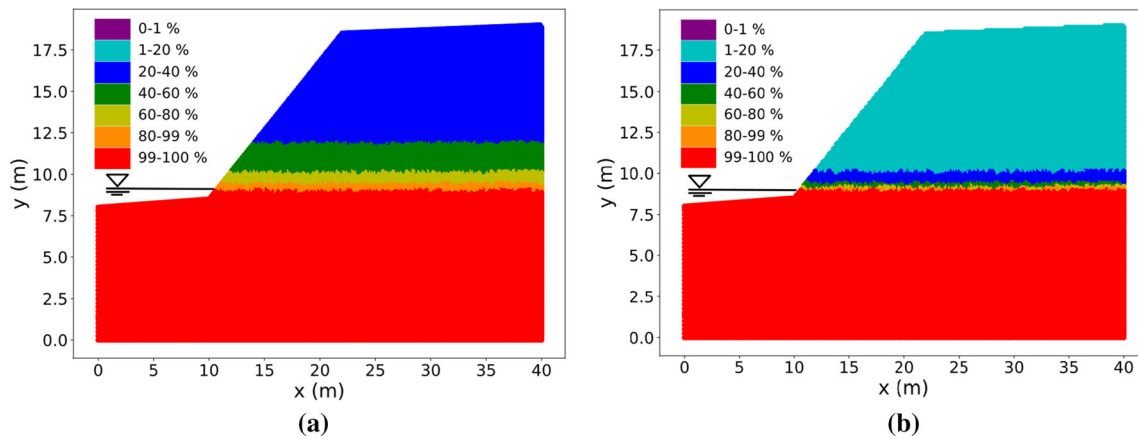
Fig. 10 Spatial variation in the soil unit weight at t=0 in **a** silty slope and **b** sandy slope
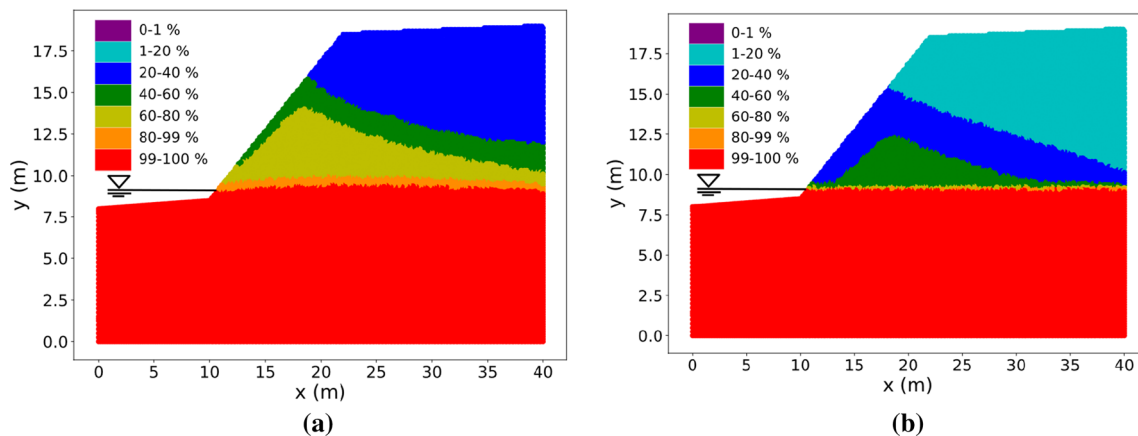

Fig. 11 Spatial variation in the saturation at t=90 days in **a** silty slope and **b** sandy slope

$t = 90$ days, respectively. In Fig. 10a, the majority of the unsaturated zone in the silty slope has a degree of saturation between "20–40%" with a unit weight of "17.4–18.4 kN/m^3." By contrast, in Fig. 10b, the dominant range of degree of saturation in the unsaturated zone of the sandy slope is "1–20%" with a soil unit weight of "16.4–17.0 kN/m^3." Figure 11 shows that the distribution of the saturation changes during the water level fluctuation. A comparison of Figs. 10 and Fig. 11 indicates that an identical level of water table might exist with different spatial saturation variations. In Fig. 11b, despite the changes in the distribution of the degree of saturation, the unsaturated unit weight in the sandy slope has a less obvious variation than that in the silty slope. To show the range of changes in the silty and sandy slopes, the degree of saturation and soil unit weight along the pass $x = 22$ m are plotted in Fig. 12a and b for $t = 0$ and $t = 90$ days, respectively. In both plots, it can be easily seen that the range of the changes for the unsaturated zone of the silty slope is greater than the sandy slope. Thus, in the sandy soil, the dry unit weight can be used in the slope stability

analysis for the unsaturated zone without causing a significant difference in the results of *FS*.

4.3 Influence of unsaturated shear strength models on *FS*

Slope stability analysis needs to be done with a soil shear strength model. In fully saturated slopes, it is common to adopt the widely accepted Mohr–Coulomb model. However, the model selection becomes more difficult and less understood when an unsaturated zone is present in the slope. To reveal the influence of unsaturated shear strength models on the *FS* results during the water level fluctuation, BS was modified with the two common unsaturated shear strength models: the Fredlund et al. [8] and the Vanapalli et al. [33].

Figure 13a and b presents the *FS* results with these two shear strength models during the water level fluctuation in the silty and sandy slopes, respectively. As can be seen, the Fredlund et al. [8] model with the assumption of $\phi^b = \phi'/2$ yielded higher values of *FS* in both the silty and sandy
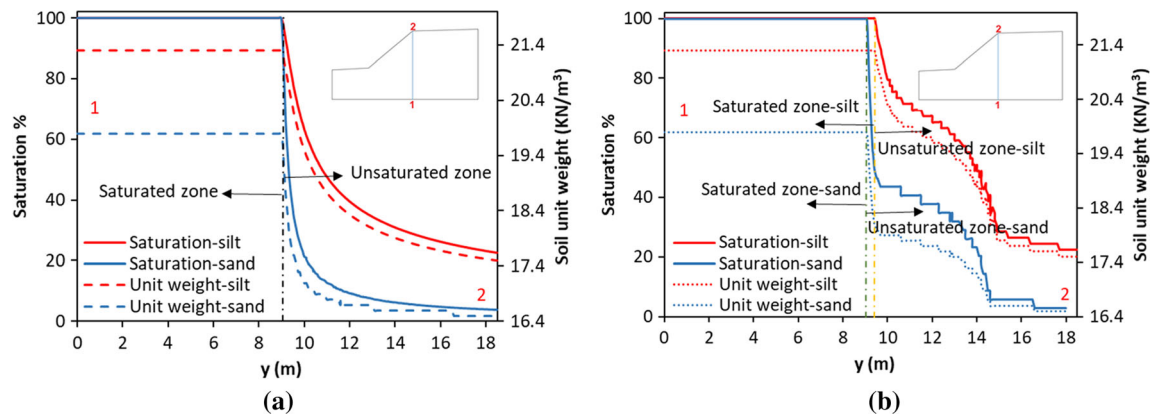
Fig. 12 Saturation and unit weight variation along the path x=22 in silty and sandy slopes at **a** t = 0 and **b** t = 90 days
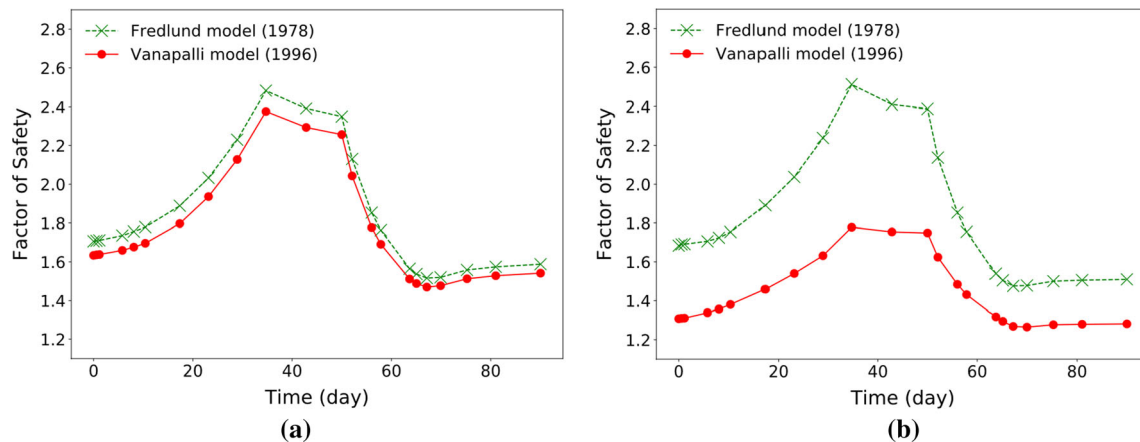

Fig. 13 Influence of two unsaturated shear strength models on *FS* results obtained from Modified BS in **a** silty slope and **b** sandy slope

slopes. This is because the Fredlund et al. [8] model neglects the spatial variation in the saturation during the transient flow, thus tends to produce a higher value for the shear strength and the *FS*. The Vanapalli et al. [33] model yielded more conservative values for the *FS* due to the consideration of the degree of saturation in the shear strength calculations. It was noticed that the critical slip surface obtained with the Fredlund et al. [8] model at a time t_i is not necessarily identical to that obtained with the Vanapalli et al. [33] model under the same geometrical, material, and boundary conditions. From Fig. 13a, it was observed in the silty slope that the *FS* values from the Fredlund et al. [8] model are 2.5% to 5% higher than the *FS* values from the Vanapalli et al. [33] model. By contrast, Fig. 13b shows that the difference between *FS* values obtained with the Fredlund et al. [8] model and the nonlinear Vanapalli et al. [33] model in the sandy slope is more significant than that in the silty slope. For the sandy slope, *FS* values computed using the Fredlund et al. [8] model are 14.6% to 28% higher than the *FS* values computed using the Fredlund et al. [33] model.

Monitoring the pore water pressure and effective degree of saturation during the water level fluctuation can help further understand the above findings. Five points in the slope (G, H, I, J, K) as shown in Fig. 3 were selected. Changes of the pore water pressure at these five points in both silty and sandy slopes during the water level fluctuation are plotted in Fig. 14. The corresponding variation in the effective degrees of saturation in sandy and silty soils is presented in Fig. 15 which are derived from Fig. 14 by applying Eq. 5. Comparing Fig. 14a and b shows that the pore water pressures in both silty and sandy slopes have similar distributions during the transient flow regardless of the oscillations in the vicinity of the water table. This is because the governing equation for the transient saturated–unsaturated flow is highly nonlinear PDE at the interface between saturated and unsaturated zones. The Fredlund et al. [8] model only incorporates the changes in the pore water pressure, U_w, as seen in Eq. 16. For this reason, the Fredlund et al. [8] model for both types of soils, i.e., sandy and silty, yields similar patterns for the *FS* results. Despite the similar pore water distribution, the distribution of effective saturation in the silty and sandy soils, Fig. 15a
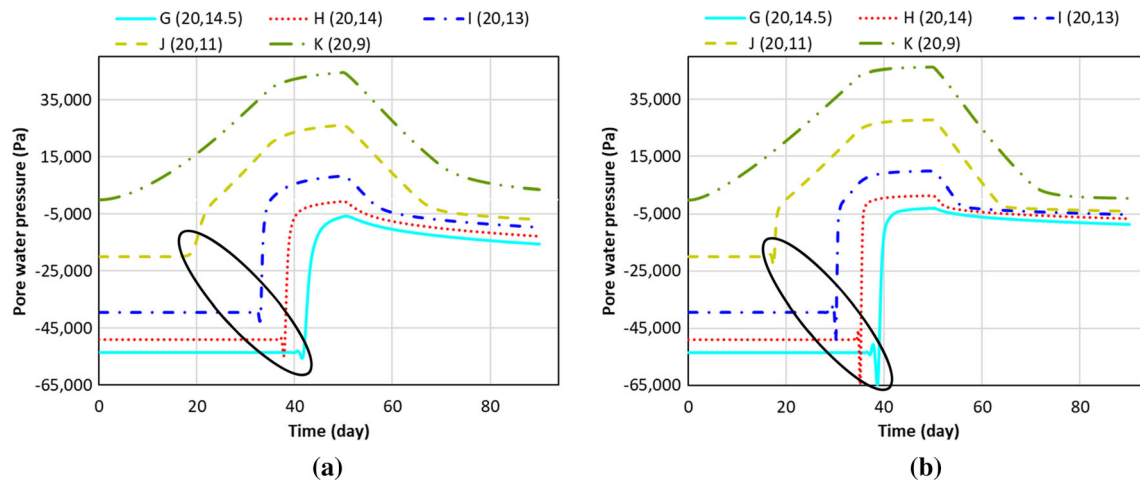
Fig. 14 Monitoring the pore water pressure during the water level fluctuation at points G, H, I, J, and K in **a** silty slope and **b** sandy slope
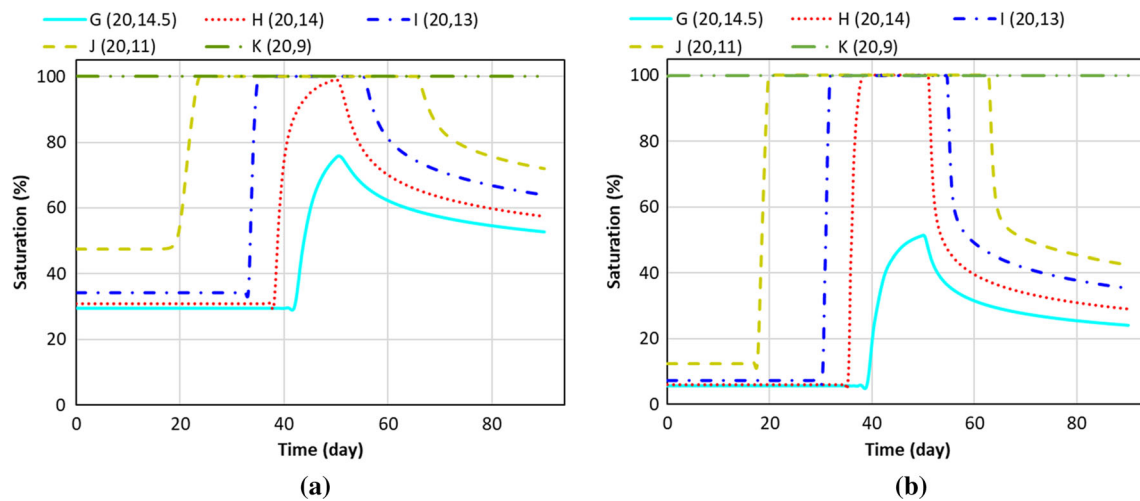

Fig. 15 Variation in the degree of saturation during the water level fluctuation at points G, H, I, J, and K in **a** silty slope and **b** sandy slope

and b, is different. Effective saturation represents the SWCC which illustrates the unique behavior of soil in the seepage process [42]. The Vanapalli et al. [33] model includes the SWCC in the computation of the FS by multiplying the degree of saturation, i.e., S_e, as seen in Eq. 17. Therefore, the FS results with consideration of the Vanapalli et al. [33] model for unsaturated shear strength seem to be more reasonable for the transient saturated–unsaturated model.

4.4 Effects of the water-level drawdown velocity on FS

It has been claimed that the reduction in stabilizing influence of the hydrostatic pressure during the drawdown is one of the major reasons for the decrease in the slope stability [22, 25]. However, this statement was made mostly from a static perspective. As a result, the possibility

that the water drawdown velocity can lead to different magnitudes and patterns of FS variations in silty and sandy slopes has not been well understood. In this study, the influence of the drawdown velocity (V_d) on the rate of the reduction in FS values of the silty and sandy slopes was investigated. For this purpose, the framework proposed in this study was used to perform analyses using two water level fluctuation profiles with different drawdown velocities. The two profiles, i.e., Case A and Case B, are plotted in Fig. 16a and b. In Case A, the water level at t = 50 days drops 6 m with the velocity of 0.3 m/day, while in Case B, the water level declines with a higher velocity of 1.0 m/day. The duration of the drawdown in Case B is 6 days which is shorter than the duration of 20 days in Case B. Figure 16a and b also presents the FS results during the water level fluctuation of Case A and Case B, respectively. For the calculation of FS, the modified BS with the Vanapalli et al. [33] model was used.
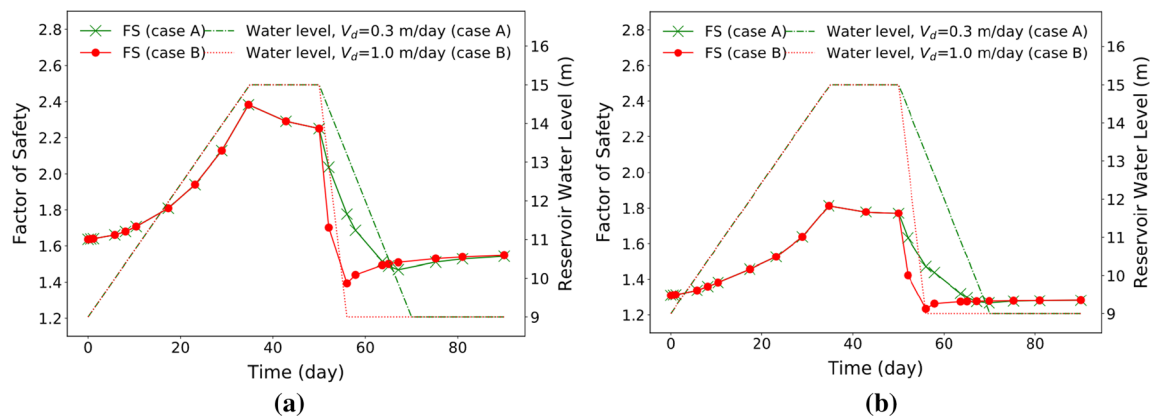
Fig. 16 Influence of the drawdown velocity on the variation in *FS* in **a** silty slope and **b** sandy slope

The *FS* results for Case B exhibit a higher rate of reduction compared to the results for Case A in both sandy and silty slopes. In Fig. 16a for the silty slope, it was observed that the *FS* decreases 34.7%, i.e., from 2.25 to 1.47, during the drawdown with the consideration of Case A. The drawdown in Case B leads to a 38.2% reduction in the *FS*, i.e., from 2.25 to 1.39. The quick drop of the water level in Case B within the shorter amount of time, 6 days, yields a more 3.5% decrease in the *FS*. By contrast, Fig. 16b for the sandy slope shows a 28.2% decrease in the *FS*, i.e., from 1.77 to 1.23, for Case A, and a 30.5% decrease in the *FS*, i.e., from 1.77 to 1.23, for case B. There is a 2.3% difference between the reductions in the *FS* value comparing Cases A and Case B. Figure 16 shows that the reduction in the stability of slopes during the water level drawdown can be even more significant for the fine-grained soils, i.e., clays, with lower hydraulic conductivities. A lower drainage rate of the pore water pressure in the silty slope increases the slope's total weight and decreases the stability of the slope.

5 Conclusion

In this study, a series of coupled seepage and slope stability analyses were conducted to investigate the influence of the water level fluctuation on the stability of the sandy and silty slopes. Two widely adopted LEMs, i.e., the BS and OMS, were modified to consider factors that were not well understood for this topic: the shear strength of the unsaturated zone, spatial variation in the soil unit weight in the unsaturated zone, and hydrostatic pressure for the partially submerged slope. Coupled analyses considering the soil unit weight variation, unsaturated shear strength models, and drawdown velocity of the reservoir yielded the following major findings that can contribute to the state of practice.

1. The decision on whether to consider the unit weight variation in the unsaturated zone in slope stability analysis needs to be made with respect to the soil type. The results clearly showed that the consideration of the soil unit weight variation does not have a noticeable effect on the *FS* of slopes consisting of a sandy soil. However, for slopes consisting of a silty soil, the *FS* values with the consideration of the soil unit weight variation are 3 to 6% lower than that without such consideration, i.e., using dry unit weight for the unsaturated zone. The comparison can be more obvious when the soil types are even further apart in the particle size axis, such as gravels and clays. Generally, for slopes consisting of mostly coarse-grained materials, the dry unit weight can be assigned to the unsaturated zone without introducing a noticeable difference in the *FS* results. Nonetheless, the consideration of a varying unit weight yielded conservative *FS* predictions in slopes containing fine-grained soils.

2. The selection of the unsaturated soil strength models can affect the *FS* calculations considerably. The degree of saturation has a substantial impact on soil shear strength. During the water level fluctuation, the Vanapalli's model (1996) can better formulate the changes of the unsaturated shear strength by including the SWCC, i.e., the term of the effective degree of saturation, in the calculations. By contrast, the Fredlund et al. [8] model with the assumption of constant $\phi^b = \phi'/2$ yielded higher values of shear strength and *FS* due to the exclusion of the relationship between the matric suction and degree of saturation. Implementing stability analysis with the assumption of Fredlund's model for the unsaturated shear strength is not suggested during the water level fluctuation because of the spatial and temporal variation in the degree of saturation.

3. The velocity of water drawdown in neighboring water bodies, such as a reservoir, was shown to have a noticeable influence on the slope stability. The slope stability generally decreases as the drawdown velocity increases, but the magnitude of the reduction in the *FS* depends on the type of soil. The reduction in the *FS* results of silty slopes is higher than that in sandy slopes. Higher values of the hydraulic conductivity help lower the groundwater table in the slope and thus increase the slope stability.

References

1. Bishop AW (1955) The use of the slip circle in the stability analysis of slopes. Geotechnique 5(1):7–17
2. Borja RI, White JA, Liu X, Wu W (2012) Factor of safety in a partially saturated slope inferred from hydro-mechanical continuum modeling. Int J Numer Anal Meth Geomech 36(2):236–248
3. Cho SE (2016) Stability analysis of unsaturated soil slopes considering water-air flow caused by rainfall infiltration. Eng Geol 211:184–197
4. Das BM (2019) Advanced soil mechanics. Crc Press, USA
5. Das BM, Sobhan K (2013) Principles of geotechnical engineering. Cengage learning, USA
6. Duong TT, Do DM, Yasuhara K (2019) Assessing the effects of rainfall intensity and hydraulic conductivity on riverbank stability. Water 11(4):741
7. Fellenius W (1936) "Calculation of stability of earth dam." Proc., Transactions. 2nd congress large dams, Washington, DC., 445–462
8. Fredlund D, Morgenstern NR, Widger R (1978) The shear strength of unsaturated soils. Can Geotech J 15(3):313–321
9. Fredlund DG, Xing A, Fredlund MD, Barbour S (1996) The relationship of the unsaturated soil shear strength to the soil-water characteristic curve. Can Geotech J 33(3):440–448
10. Fredlund M, Lu H, Feng T (2011) Combined seepage and slope stability analysis of rapid drawdown scenarios for levee design. Geo-Front: Adv Geotech Eng. https://doi.org/10.1061/41165(397)163
11. Froude MJ, Petley D (2018) Global fatal landslide occurrence from 2004 to 2016. Nat Hazard 18:2161–2181
12. Gofar N, Rahardjo H (2017) Saturated and unsaturated stability analysis of slope subjected to rainfall infiltration. EDP Sci 101:05004 (MATEC Web of Conferences)
13. Huang, W., Leong, E., and Rahardjo, H. "Simplified stability analysis of unsaturated soil slopes under rainfall." Proc., Proc., 7th Int. Conf. on Unsaturated Soils (UNSAT 2018). Hong Kong: Hong Kong Univ. of Science and Technology
14. Iqbal, J., Tu, X., and Gao, W. (2019). "The impact of reservoir fluctuations on reactivated large landslides: a case study." *Geofluids*, 2019.
15. Ishak M, Zolkepli M (2016) Exploration of methods for slope stability analysis influenced by unsaturated soil. Electron J Geotech Eng 21:5627–5641
16. Jeong S, Lee K, Kim J, Kim Y (2017) Analysis of rainfall-induced landslide on unsaturated soil slopes. Sustainability 9(7):1280
17. Jiao Y-Y, Zhang H-Q, Tang H-M, Zhang X-L, Adoko AC, Tian H-N (2014) Simulating the process of reservoir-impoundment-induced landslide using the extended DDA method. Eng Geol 182:37–48
18. Li S, Sun Q, Zhang Z, Luo X (2018) Physical modelling and numerical analysis of slope instability subjected to reservoir impoundment of the Three Gorges. Environ Earth Sci 77(4):138
19. Li X, Zhao C, Hölter R, Datcheva M, Alimardani Lavasan A (2019) Modelling of a large landslide problem under water level fluctuation—model calibration and verification. Geosciences 9(2):89
20. Liang C, Jaksa M, Ostendorf B, Kuo Y (2015) Influence of river level fluctuations and climate on riverbank stability. Comput Geotech 63:83–98
21. Liu J, Yang C, Gan J, Liu Y, Wei L, Xie Q (2017) Stability analysis of road embankment slope subjected to rainfall considering runoff-unsaturated seepage and unsaturated fluid–solid coupling. Int J Civil Eng 15(6):865–876
22. Liu Q, Li J (2015) Effects of water seepage on the stability of soil-slopes. Procedia IUTAM 17:29–39
23. Liu ZL (2018) "Multiphysics in Porous Materials" Multiphysics in porous materials. Springer, Berlin
24. Maina-Gichaba C, Kipseba EK, Masibo M (2013) "Overview of landslide occurrences in Kenya: causes, mitigation, and challenges." Developments in earth surface processes, Elsevier, USA
25. Oya, A., Bui, H. H., Hiraoka, N., Fujimoto, M., and Fukagawa, R. (2015). "Seepage flow-stability analysis of the riverbank of Saigon river due to river water level fluctuation." *arXiv preprint* arXiv:1505.07747.
26. Paronuzzi P, Rigo E, Bolla A (2013) Influence of filling–drawdown cycles of the Vajont reservoir on Mt. Toc slope stability. Geomorphology 191:75–93
27. Petley D (2012) Global patterns of loss of life from landslides. Geology 40(10):927–930
28. Rahardjo H, Leong EC, Deutscher MS, Gasmo JM, Tang S (2000) Rainfall-induced slope failures. Geotech Eng Monogr 3:86
29. Sethi R, Di Molfetta A (2019) Groundwater engineering: a technical approach to hydrogeology. Springer, Berlin
30. Song K, Yan E, Zhang G, Lu S, Yi Q (2015) Effect of hydraulic properties of soil and fluctuation velocity of reservoir water on landslide stability. Environ Earth Sci 74(6):5319–5329
31. Sun D-M, Zang Y-G, Semprich S (2015) Effects of airflow induced by rainfall infiltration on unsaturated soil slope stability. Transp Porous Media 107(3):821–841
32. van Genuchten MT (1980) A closed-form equation for predicting the hydraulic conductivity of unsaturated soils 1. Soil Sci Soc Am J 44(5):892–898
33. Vanapalli S, Fredlund D, Pufahl D, Clifton A (1996) Model for the prediction of shear strength with respect to soil suction. Can Geotech J 33(3):379–392
34. VandenBerge DR, Duncan JM, Brandon TL (2015) Limitations of transient seepage analyses for calculating pore pressures during external water level changes. J Geotech Geoenviron Eng 141(5):04015005
35. Verruijt A (1995) Computational geomechanics. Springer, Berlin
36. Wang H, Xu W, Xu R, Jiang Q, Liu J (2007) Hazard assessment by 3D stability analysis of landslides due to reservoir impounding. Landslides 4(4):381–388

37. Wang W, Griffiths D (2020) Analysis of the critical pool level of partially submerged slopes. Int J Numer Anal Meth Geomech 44(3):405–417

38. Whitman RV, Moore PJ (1963) Thoughts concerning the mechanics of slope stability analysis, Department of Civil Engineering, Massachusetts Institute of Technology

39. Wu Y, Miao F, Li L, Xie Y, Chang B (2017) Time-varying reliability analysis of Huangtupo Riverside No. 2 Landslide in the Three Gorges Reservoir based on water-soil coupling. Eng Geol 226:267–276

40. Zhang L, Fredlund DG, Fredlund MD, Wilson GW (2014) Modeling the unsaturated soil zone in slope stability analysis. Can Geotech J 51(12):1384–1398

41. Zhang M, Dong Y, Sun P (2012) Impact of reservoir impoundment-caused groundwater level changes on regional slope stability: a case study in the Loess Plateau of Western China. Environmental earth sciences 66(6):1715–1725

42. Zhang Y, Song Z, Weng X, Xie Y (2019) "A new soil-water characteristic curve model for unsaturated loess based on wetting-induced pore deformation." Geofluids, 2019